European Water 89: 81-99, 2025.

Exploring the role of coloured noise in modelling short- and long-term dependence structures in monthly streamflows across Ontario, Canada

Shirin Studnicka and Umed Panu*

Department of Civil Engineering, Lakehead University, Thunder Bay, ON, Canada
* *e-mail: uspanu@lakeheadu.ca*

Abstract: Nonstationary hydrological behaviour poses significant challenges in water resources management. Understanding its temporal structure is essential, and scaling behaviour is crucial, as it directly indicates the colour of noise (pink, brown, or black), and thus helps describe the memory behaviour of such systems. For rigorous quantification of the scaling behaviour, a new approach analyzing jumps observed in the power spectral density at specific frequencies is proposed. The study investigates the relationship between the scaling exponent (α) and the Hurst exponent (H), which is typically invoked in hydrology to quantify the memory of a system. To quantify the scaling behaviour of monthly streamflow across Ontario, Canada, initially, all continuous hydrometric stations were selected. All those hydrometric stations having data gaps exceeding 24 months were excluded, thus resulting in a total of 143 hydrometric stations for analysis. The results revealed the presence of brown noise in 2 stations, pink noise in 39 stations, and black noise in 101 stations. A linear relationship between exponents α and H for the pink noise is expressed by $\alpha = 0.1156H + 1.6258$, and for the black noise by $\alpha = 2.0396H + 1.4718$. In other words, the scaling behaviour of systems exhibiting pink noise shows less dependence on the Hurst exponent (i.e., a gradual slope of 0.1156), thereby suggesting a shorter memory than systems exhibiting black noise. Furthermore, capturing immediate (short-term) correlations is more important in such systems, exhibiting black noise that is highly influenced by past distant events (i.e., long-term memory, a hallmark of the strong presence of the Hurst exponent with a sharp slope of 2.0396). Thus, the preservation of the long-term temporal structure of the system is crucial for accurate modelling.

Key words: Scaling exponent; Hurst exponent; Power spectral analysis; $1/f^{\alpha}$ Noise; Power law; Coloured Noise; Persistence; Short-term Correlations.

1. INTRODUCTION

Scaling behaviour in streamflow time series refers to how, over time, patterns and statistical properties at different temporal scales change. Investigating scaling behaviour provides a powerful tool for understanding, modelling, and managing hydrological processes. The scaling behaviour of a system is not dependent on the specific point in time. For example, if an original time series is shifted by a one-time step, a bias may be introduced compared to the original series. However, the correlation structure and scaling behaviour remain unchanged in the same time series, as these properties are intrinsic to the data and independent of the temporal shift. The concept governing such behaviour suggests that different time scales may exhibit similar or complementary statistical properties, indicating multi-scale correlations and persistent memory in the system. In hydrology, such a characteristic of streamflow is often quantified using the *Hurst exponent* (Hurst, 1951; Fiering & Bund, 1971; Klemeš, 1974; Boes & Salas, 1978; Panu & Unny, 1980a; Salas et al., 1980; Stedinger & Taylor, 1982; Sharma et al., 1997; Koirala et al., 2011; Szolgayova et al., 2014; Legates & Outcalt, 2022; Suman et al., 2023).

The Hurst exponent (H) is a widely accepted concept in hydrology to measure the persistence or long-term memory of a time series and is often used as a criterion to evaluate the performance of hydrological models (Jackson, 1975; Panu & Unny, 1980b; Koutsoyiannis, 2003; Livina et al., 2007; Zhang et al., 2009; Markonis et al., 2018; Piran & Panu, 2023; Studnicka & Panu, 2025). When synthesizing or forecasting streamflow, the model must capture the long-term dependencies exhibited in streamflow time series (Fiering & Bund, 1971; Panu & Unny, 1980b, 1980c; Salas et al., 1980). However, the concept of scaling behaviour in hydrology has not yet been extensively

explored in the literature (Livina et al., 2007; Stoyanov et al., 2011; Telesca et al., 2012; Kim et al., 2016).

To quantify the scaling behaviour of a system, it is widely accepted that Power Spectrum Analysis (PSA) represents a powerful tool to determine the scaling behaviour of time series (Blöschl & Sivapalan, 1995; Dolgonosov et al., 2008; Telesca et al., 2012; Thompson & Katul, 2012; Kim et al., 2016; Wen & Liu, 2016; Gu et al., 2020). In PSA, the power of a signal at various frequencies is plotted on a log-log graph. If the power spectrum follows a $(1/f^{\alpha})$ form then it is indicative of a scaling behaviour with a scaling exponent (or power-law exponent) of α (Dooley & Van de Ven, 1997; Telesca et al., 2012).

To estimate α, a key challenge in the hydrology literature is the potential variability of α across different frequencies (Telesca et al., 2012; Thompson & Katul, 2012; Kim et al., 2016). Such a variability implies that α may either remain constant or change depending on the frequency. The variability in α across frequencies complicates the estimation process and presents a significant challenge in hydrological studies (Thompson & Katul, 2012; Gu et al., 2020).

Telesca et al. (2012) analyzed the power spectrum of monthly streamflow in Spain using the high-frequency band (frequencies higher than the annual cycle). They fitted a line to the power spectrum on a log-log graph using the least squares method, finding that the scaling exponent in this band indicates that streamflow exhibits persistence on timescales shorter than one year, varying between approximately 0.9 and 1.4 for most streamflow time series. Similarly, Thompson and Katul (2012) determined the slope of a power spectrum by focusing on the high-frequency regime and observed that, despite breaks in scaling and shifts in the intercepts of the spectra with variations in certain parameters, the slopes at higher frequencies remained consistent. In another study, Kim et al. (2016) identified two distinct scaling regimes in hydrologic time series and computed a cross-point using segmented linear regression on the power spectrum in a log-log space, denoting the low-frequency slope and the high-frequency slope, with an average slope to estimate α. Subsequently, the estimate of α was utilized by Kim et al (2016) to recognize and diagnose the colour of the noise, which also reflects the memory of the system.

When the scaling exponent, $\alpha = 0$, a time series exhibits white noise, characterized by random fluctuations with no correlation (and therefore no memory). In contrast, a scaling exponent in the range $0 < \alpha < 2$ corresponds to pink noise. For the scaling exponent, $\alpha = 2$, the behaviour is identified as brown noise or Brownian motion. Finally, for $\alpha > 2$, the series represents a black noise. Each of these coloured noises is considered to possess unique characteristics, such as the Pink Noise (also known as mean revert, which means that if the series is high at one point, it is likely to be low at the next time step, and vice versa). Brown noise is the overtime accumulation of white noise; therefore, differenced brown noise at lag-one becomes white noise. Finally, black noise indicates a low-frequency dominance structure (Dooley & Van de Ven, 1997; Sun et al., 2007; Stoyanov et al., 2011; Chen et al., 2013; Souza & Assireu, 2016).

In signal processing, pink noise is characterized as anti-persistent ($0 < H < 0.5$) and as having a short memory (Dooley & Van de Ven, 1997; Balabana & Lub, 2018). However, in hydrological time series, pink noise is characterized as persistent and having a long memory, though shorter than black noise (Kim et al., 2016). Such a difference arises due to the nature of a system. In finance, a peak, such as a sudden rise in stock prices, may be followed by a contrasting movement (e.g., a drop), influenced significantly by human behaviour and financial market dynamics. This anti-persistent behaviour reflects the tendency of a system to revert to its mean value over *short periods*. Conversely, in hydrology, extreme events such as floods are less likely to be *immediately* followed by opposite extremes, like severe droughts. Even if such contrasts occur, they are not representative of the long-term behaviour in hydrological systems. Instead, hydrological systems often exhibit consistent behaviour over extended periods, resulting in the observed persistence in hydrological time series.

Several studies have attempted to analyze the scaling properties and underlying statistics (Dooley & Van de Ven, 1997; Rodriguez-Iturbe & Rinaldo, 1997; Bullmore et al., 2001; Koscielny-Bunde et al., 2006; Balabana & Lub, 2018). The existence of a relationship between α and H was

first highlighted by Gallant et al. (1994) and Blöschl and Sivapalan (1995), as both describe the concept of memory in a time series.

For stationary series, Koscielny-Bunde et al. (2006) discussed that the autocorrelation function (ACF) decays with lag-k following $ACF(k) \sim k^{1-\alpha}$, where α =2H-1; while for non-stationary series α =2H+1. It is widely accepted that in hydrologic time series 0.5 < H < 1 (Salas et al., 1980). Based on such an observation, it can be concluded that the expression 0 < 2H-1 < 1 holds, and similarly, 2 < 2H+1 < 3. These boundaries imply that stationary series are characterized by pink noise 0 < α < 1 (where α = 2H-1), and nonstationary series are characterized by black noise 2 < α < 3 (where α = 2H+1).

Considering that the monthly streamflows are highly non-stationary (Panu & Unny, 1980b; Salas et al., 1980; Rhif et al., 2019), it is expected that monthly streamflows are characterized as predominantly Black noise (based on 2 < 2H+1 < 3). However, an investigation into the scaling properties of monthly streamflow (1950–2005) in Spain, using the PSA and the detrended fluctuation analysis at 11 gauging stations in the Ebro Basin, revealed characteristics of pink noise (Telesca et al., 2012). This implies that, firstly, the α-H relationship for non-stationary series needs further investigation in hydrology. Secondly, monthly streamflow may exhibit all types of coloured noise (Cuddington & Yodzis, 1999), which is further discussed in section 2.2.1.

Therefore, this study aims to investigate the presence of different types of coloured noise by simplifying and developing a novel approach to PSA in monthly streamflow and to establish the relationship between the scaling exponent (α) and the Hurst exponent (H) for Ontario streams.

2. MATERIALS AND METHODS

2.1 Study area

Out of 1122 hydrometric stations in Ontario, discontinued stations were excluded because their outdated data sets may not account for the effects of urbanization on the scaling exponent (Kim et al., 2016). Additionally, continuous hydrometric stations with data gaps exceeding two years (24 monthly observations) were excluded, as gap-filling could potentially affect the Hurst coefficient.

As a result, 143 hydrometric stations were chosen, and relevant hydrologic information of the selected hydrometric stations is presented in Appendix A. Furthermore, Figure 1 presents the geographical distribution of selected hydrometric stations in Ontario.

2.2 Methodology

This study develops new insights into the characteristics of various noises and their interplay towards the presence or absence of short- or long-term memory in the Ontarian monthly streamflow through investigations into the scaling behaviour of the power spectrum density in the section to follow and onwards develops a relationship between the scaling exponent "α" and the Hurst exponent "H".

2.2.1 Power spectrum analysis

Time series can often be viewed as a combination of multiple sinusoidal waves with varying frequencies or periods. Based on such an assumption, a time series, when analyzed in the frequency domain using the Fourier transform, the spectral density function describes the contribution of each frequency to the overall variance of the series. The Fourier transform of a hydrologic time series, $x(t)$, into its frequency domain representation, G(f), is expressed as follows:

$$\mathrm{G(f)} = \int_{-\infty}^{+\infty} \mathrm{x(t)e^{-2\pi ift}dt} \quad (1)$$

where t represents time, f is the frequency, and $i = \sqrt{-1}$. A PSA is typically used to assess the periodic strength in a time series across various timescales, such as monthly, annual, and decadal. However, the existence of a linear relationship between a frequency and a power spectrum on a log-log scale indicates scale invariance in the temporal domain. Such a relationship is expressed as follows:

$$P(f) \propto 1/f^{\alpha} \tag{2}$$

where *P(f)* is the power spectral density (PSD) at that frequency, and the scaling exponent α is the slope of the line of best fit on a log-log plot. This scale-invariance characteristic of the power spectrum is known as $1/f^{\alpha}$ Noise, where the colour of the noise varies based on the value of α.

In analyzing the scaling behaviour of streamflow time series, previous studies have utilized a cross-point in frequency to divide different regimes of streamflow (Telesca et al., 2012; Thompson & Katul, 2012; Kim et al., 2016). Likewise, a cross-point in this study is defined as 1 year, as utilized by Telesca et al. (2012) for monthly streamflow. Therefore, for a frequency window of f >1/12 months (= 0.833 months^{-1}) (1 year), the power law can be analyzed.

In this window of f > 0.833 months^{-1}, Telesca et al. (2012) observed notable jumps at both 12- and 6-month intervals in the power spectrum of monthly streamflow data. They ascribed these peaks in the power spectrum to the frequencies at which cycles and patterns dominate. Such an observation was further investigated in more detail by Wen and Liu (2016), who also concluded that oscillatory patterns in a signal appear as distinct peaks in the PSD at the corresponding oscillation frequencies. The height and sharpness of such distinct peaks depend on the amplitude and purity of oscillations.

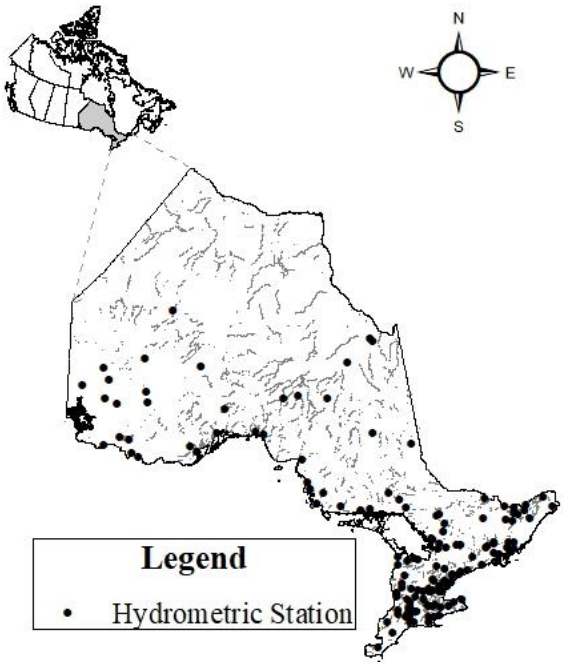

Figure 1. Spatial distribution of hydrometric stations within the study area.

Considering jumps in the PSD correspond to frequencies where certain patterns dominate, it can be expected that a jump will occur at the frequency of 12-month intervals, as this represents the frequency at which a hydrological cycle repeats. Additionally, if there are sub-patterns within the cycle, jumps can be expected at frequencies that match the durations of these sub-patterns. Telesca et al. (2012) reported two jumps at frequencies of f = 1/12 and f = 1/6 months^{-1}. The presence of different seasons (2, 3 and maybe 4) and sub-patterns within the monthly streamflow has been discussed by Panu and Unny (1980a); therefore, it is reasonable to expect peaks in PSD at frequencies corresponding to fractions of a cycle, such as 6 months, 4 months, 3 months, and 2

months. Figure 2 presents a conceptual diagram of PSD for monthly streamflow, where, within a cycle of 12 months, there exist different seasons and sub-patterns. The points labelled in Figure 2, corresponding to frequencies of f = 0.0833, 0.1667, 0.25, 0.3333, and 0.5, represent periods of 12 months, 6 months, 4 months, 3 months, and 2 months, respectively. At each of these frequencies, a notable increase or 'jump' in PSD is anticipated, which is consistent with observations reported by (Telesca et al., 2012; Kim et al., 2016).

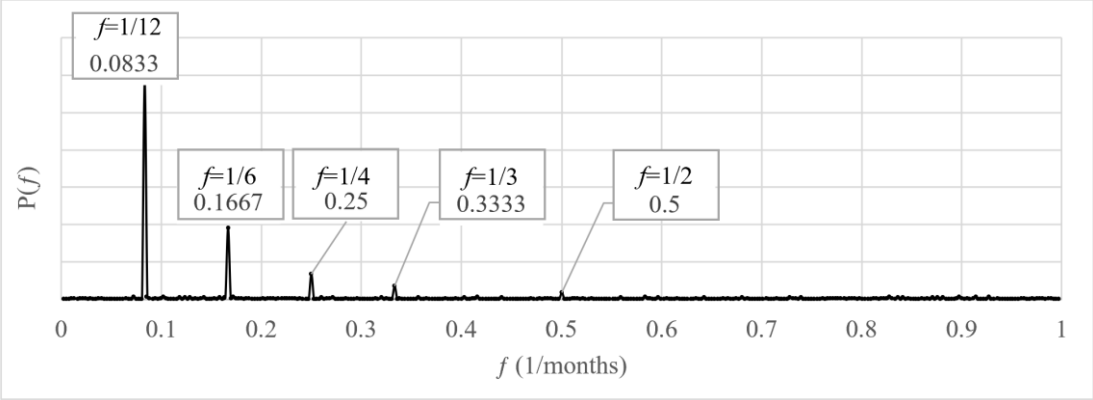

Figure 2. A PSD plot of a hypothetical monthly streamflow time series.

Should the power spectrum be expected to follow its scale-invariance characteristic of $1/f^{\alpha}$ Noise, then the rule for frequencies f > 0.0833, as recommended by Telesca et al. (2012), is that each of these observed jumps should also align with the relationship of $1/f^{\alpha}$.

Based on the foregoing discussion, in the case of monthly streamflow data, a jump in the PSD at a certain frequency indicates dominant patterns within the time series. Therefore, focusing on such jumps, where dominant patterns are most pronounced, can lead to a more accurate estimation of the scaling exponent, α. Such considerations, in turn, enhance the estimation of the Hurst coefficient, H, in our quest to adequately account for both short-term and long-term dependence in hydrologic data series for improved modelling practices. It is in this vein that this study proposes a new methodology, as illustrated in Figure 3, to isolate jumps in PSD, which in turn, imbue the $1/f^{\alpha}$ model to all such frequencies or patterns. By isolating jumps in PSD, and considering $P(f) \propto 1/f^{\alpha}$, the logarithm of both sides will be

$$\mathrm{Log}\big(\mathrm{P(f)}\big) = \mathrm{Log1} - \mathrm{Log}\,(\mathrm{f}^{\alpha}) \tag{3}$$

Therefore,

$$\mathrm{Log}\big(\mathrm{P(f)}\big) = -\,\alpha\,\mathrm{Log}\,(\mathrm{f}) + \mathrm{C} \tag{4}$$

This is used to describe the line of best fit to high-frequency points in a log-log plot, as shown in Figure 3. In Eq. 4, the constant C serves as a vertical shift in the log-log plot.

2.2.2 Colour determination of noise

The scaling exponent, α, determines the colour of noise and describes several behavioural characteristics of a time series as summarized in Table 1. It is to be noted that, as indicated in Table 1, the black noise is characterized by low-frequency dominance. Since the focus of this study is on high frequencies above 0.0833 months^{-1} and hence when analyzing a signal with a frequency window of f > 0.0833 months^{-1}, any classification as black noise implies that the lowest frequency in this range (0.0833 months^{-1}) dominates. Consequently, the high PSD value at this frequency results in a steeper slope in the log-log PSD plot, leading to a scaling exponent (α) greater than 2.

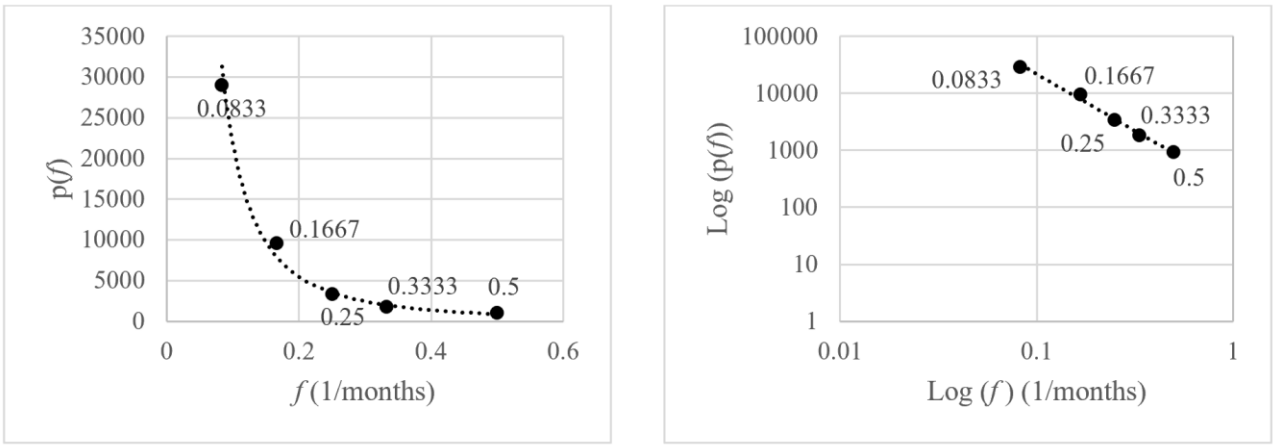

Figure 3. Depiction of isolated jumps in the PSD of a hypothetical monthly streamflow time series: (a) a linear scale and (b) a log-log scale.

Table 1. Categorization of various types of noises based on values of the scaling exponent "α".

Scaling Exponent, "α"	Noise Type	Behaviour	Memory
$\alpha = 0$	White	Random	No Memory
$0 < \alpha < 2$	Pink	Mean Reverting	Long-term memory*
$\alpha = 2$	Brown	Brownian Motion Process	No long-term memory (independent increments): Changes over non-overlapping time intervals are independent
$\alpha > 2$	Black	Structured with Low-frequency Dominance	Long-term memory**

Note: *Pink noise and **black noise both exhibit memory; however, pink noise has a shorter memory compared to black noise. In financial literature, pink noise is often ascribed to having a short memory, whereas in hydrologic studies, it is characterized by a long memory. The pink noise does possess memory, but its memory is not as persistent as that of the black noise.

To further realize and recognize the difference between white, pink, brown and black noise, various types of noise were randomly generated, and corresponding PSA were conducted as exhibited in Figure 4. This figure depicts the random generation of different coloured noises—white, pink, brown, and black—along with their corresponding PSD as well as log-log PSD plots. A line of best fit was obtained at frequencies greater than 0.0833 months^{-1}, and the corresponding equation is also displayed, whereby attesting and asserting the colour of the generated noise. For clarity, it is noted that the PSA here was not conducted by isolating peaks, as these were known to be pure-coloured noises and hence without cycles, such that there exist no jumps in their PSD.

Additionally, the combined signal (i.e., a summation of the four coloured noise types) is presented along with its log-log PSD. The combined signal exhibits a value of 0.556 for the scaling exponent "α", thereby placing it in the pink noise category. Irrespective of such a categorization, the signal demonstrates characteristics of all coloured noises, as the signal was obtained by adding various noises.

2.2.3 Hurst exponent

Hurst (1951) introduced a pioneering method for characterizing long-term persistence in time series, known as Rescaled Range (R/S) analysis, which quantifies the self-similarity and long-range dependence in a process. The procedure to estimate the Hurst exponent, H, follows several steps, as outlined below.

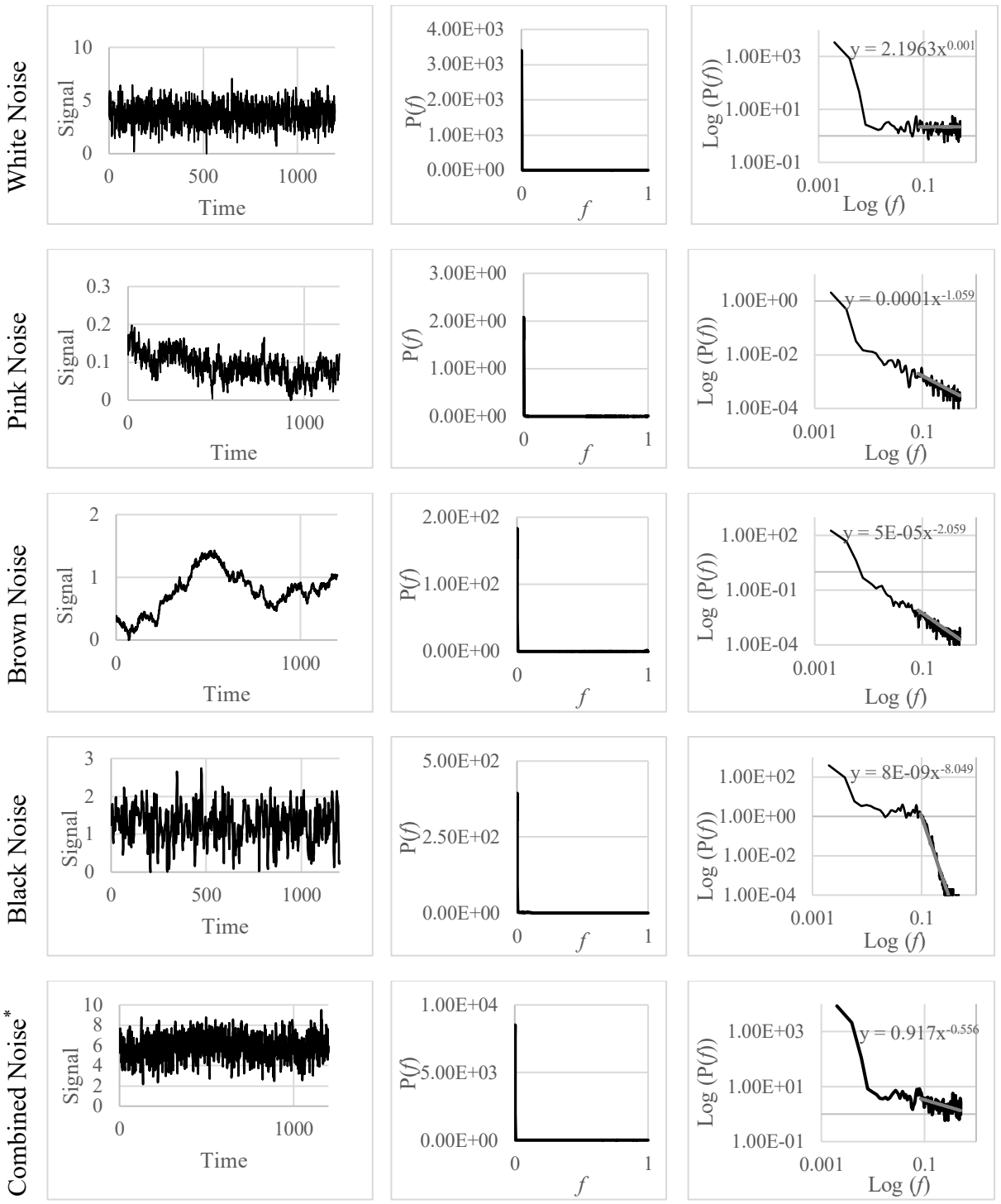

Note: *Combined signal comprises White Noise + Pink Noise + Brown Noise + Black Noise.

Figure 4. White, pink, brown, black, and combined noise signals are shown in (a) Time series representation, (b) PSD, and (c) PSD on a log-log scale.

Step-1: Segmentation: The time series of y[n] is broken up into equally sized, non-overlapping subseries of length s, denoted as

$$Y_s = \{y_{s_m}[n] \mid 1 \leq m \leq N_s\} \tag{5}$$

where y[n] is the original time series value at time step n (streamflow in m³/s), s is the length of each segment in number of time steps, m is the segment index, N_s is the total number of segments, and $y_{s_m}[n]$ is the k^{th} segment of $y[n]$, containing s consecutive values.

Step-2: Range Calculation: For each segment, m, of length s, the range $R_{m,s}$, which is the difference between the maximum and minimum values within the segment being calculated:

$$R_{m,s} = \max[y_{s_m}] - \min[y_{s_m}] \tag{6}$$

Step-3: Variance Calculation: The variance $S_{m,s}$ of the original time series values within each segment, m, of length s, is computed by:

$$S_{m,s} = \sigma_x[y_{s_m}] \tag{7}$$

Step-4: Mean Values: The mean values of the range R_s and the standard deviation S_s across all segments are determined as follows:

$$\bar{R}_s = \frac{1}{N_s}\sum_{m=1}^{N_s} R_{m,s} \tag{8}$$

$$\bar{S}_s = \frac{1}{N_s}\sum_{m=1}^{N_s} S_{m,s} \tag{9}$$

Step-5: Ratio and Scaling: The ratio $\bar{R}_s/\bar{S}_s$ exhibits a power-law scaling as a function of segment length s, which can be described by the equation:

$$\frac{\bar{R}_s}{\bar{S}_s} = S^H \tag{10}$$

where H is the Hurst exponent.

3. RESULTS AND DISCUSSION

Due to space limitations, a single station was randomly selected for each of the coloured noise types, and the corresponding results have been presented and discussed.

Figure 5 presents the PSD of Jock River (02LA007), Basswood River (05PA012), and English River (05QA002), with labelled jumps. As observed, at f = (1/fraction of a cycle), distinct jumps appear in the power spectrum. Notably, similar increases in the power spectrum have also been observed at all other stations (Appendix A). Beyond the value of f = 0.5, there is a noticeable increase in the power spectrum, and because of this increase, the analysis is limited to the range [0.0833 < f < 0.50]. These jumps in the power spectrum, corresponding to frequencies of 1/12, 1/6, 1/4, 1/3, and ½ months, are isolated and plotted in Figure 6, along with the fitted power-law functions and their corresponding R^2 values.

It is apparent from the values of 1.574, 2.008, and 2.6 (Figure 6) that the scaling exponent, α, respectively exhibits characteristics of pink, brown, and black noise for the Jock River (Figure 6a), Basswood River (Figure 6b), and English River (Figure 6c).

The presence of brown noise among 143 stations posed a challenge, as α values between 1.9 and 2.1 can also be rounded to 2, thus classifying them as brown noise. Table 2 presents 8 stations with alpha values ranging from 1.9 to 2.1.

Given that when brown noise is differenced at lag 1 becomes white noise (Dooley & Van de Ven, 1997), it is expected that the autocorrelation function (ACF) at lag 1 will be zero. As shown in Table 2, only two stations exhibit such characteristics: Basswood River near Winton (05PA012) with an α value of 2.008 and an ACF (1) of the differenced series of 0.003, and Black Sturgeon

River at Highway No. 17 (02AC002) with an α value of 2.048 and an ACF (1) of the differenced series of - 0.002.

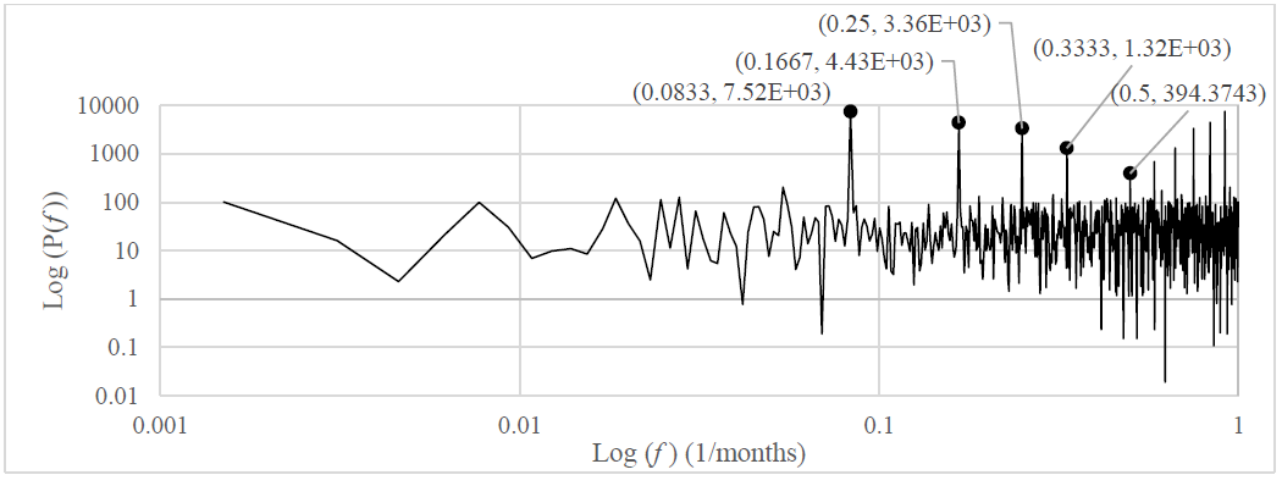

(a)

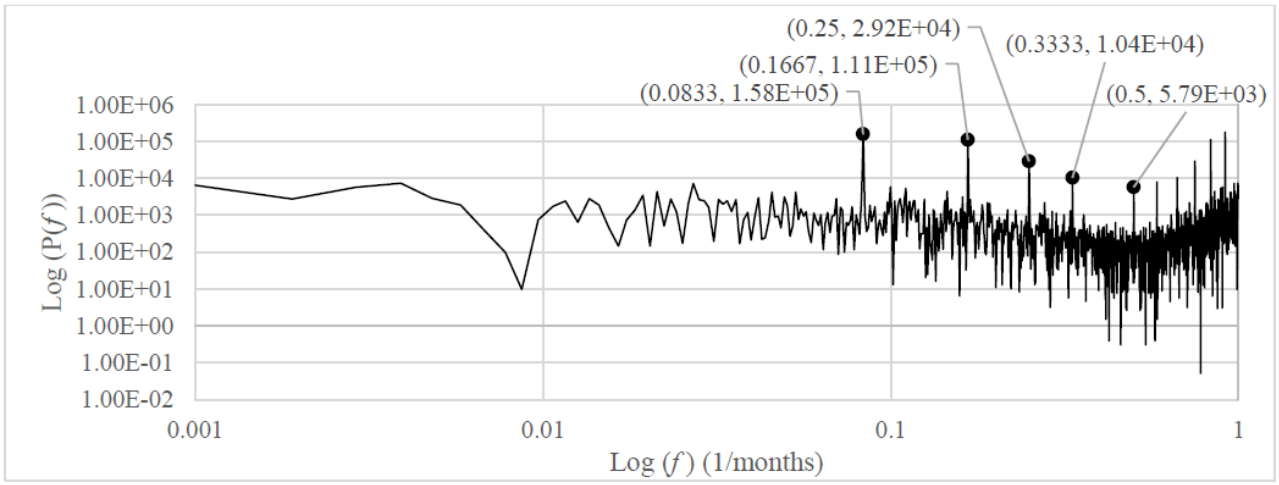

(b)

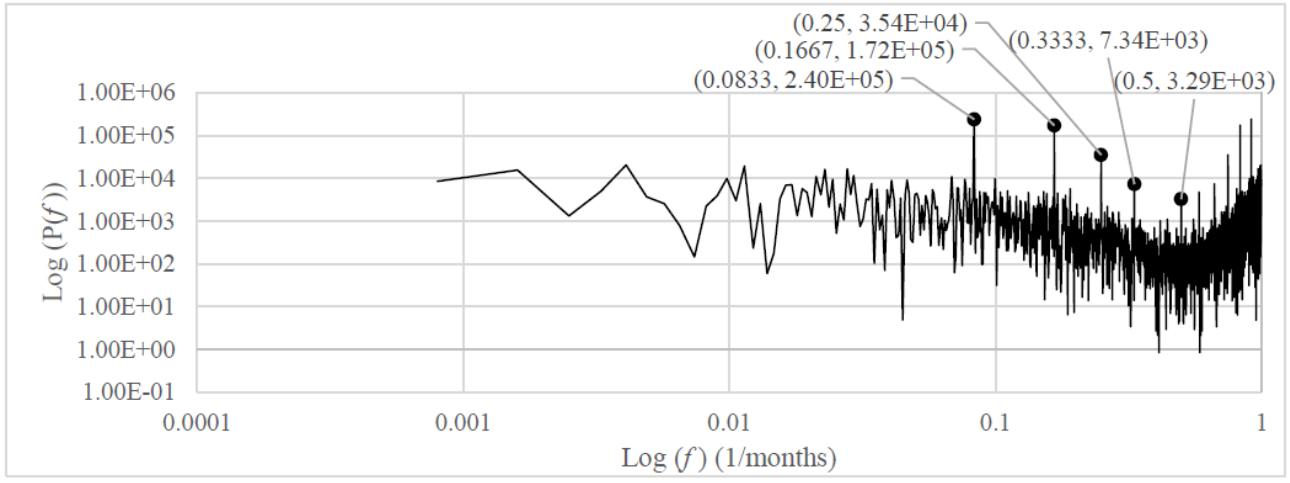

(c)

Figure 5. PSD of rivers with labelled Jumps: (a) Jock River, (b) Basswood River, and (c) English River.

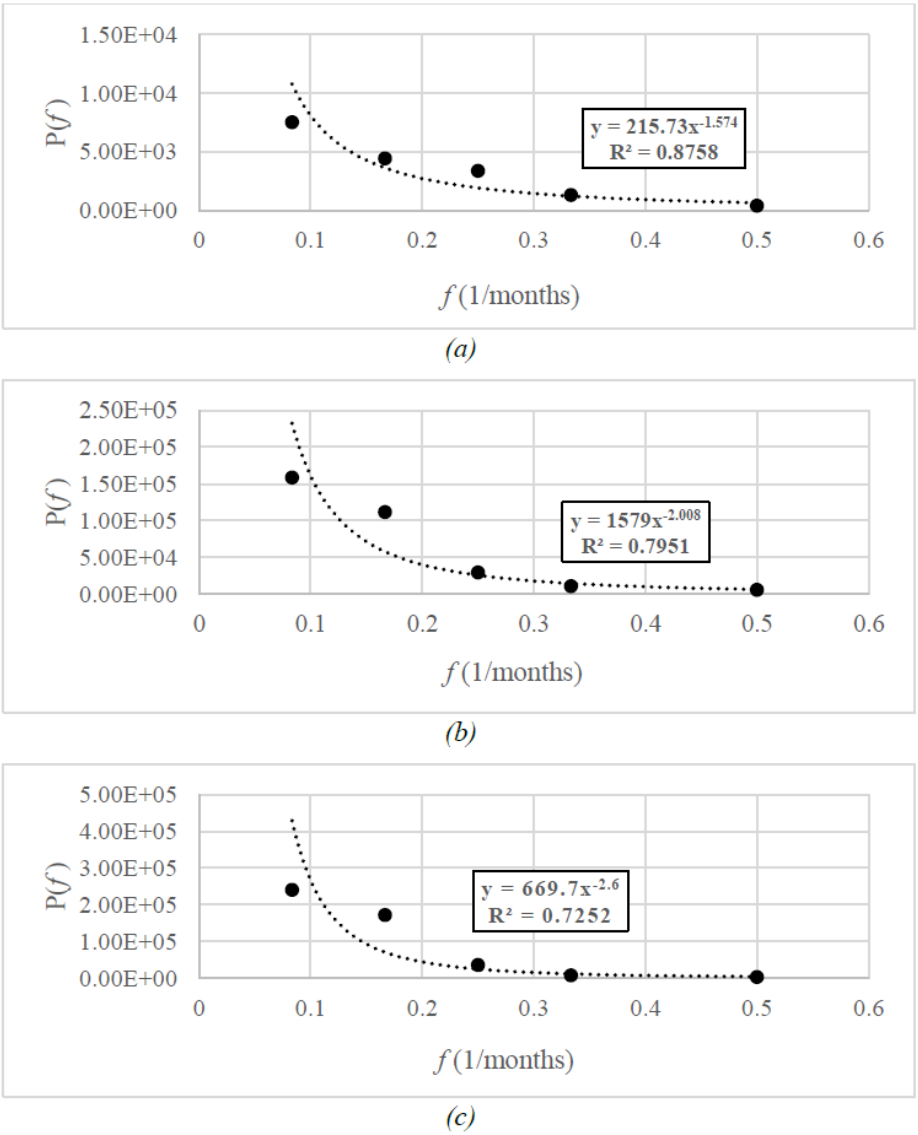

Figure 6. Isolated jumps in PSD of rivers along with the fitted exponential function: (a) Jock River, (b) Basswood River, and (c) English River.

Therefore, only two stations are characterized as brown noise, 39 as pink noise, and the remaining 102 as black noise, as shown in Figure 7.

Once stations with different levels of noise were identified, the Hurst coefficient, as explained in section 2.2.3, was obtained. Figure 8 presents all the stations with H values on the x-axis and the scaling exponent α values on the y-axis: (a) without separating the different coloured noise, and (b) with separating the coloured noise.

Table 2. Summary of stations exhibiting values of the scaling exponent, α, in the range of 1.9 and 2.1 for the existence of brown noise.

Station Name	**Scaling Exponent (α)**	**ACF (1) of a differenced series (d = 1)**
Black River near Actinolite	1.958	-0.18074
Nagagami River at Highway No. 11	1.963	-0.09993
Black River near Washago	1.98	-0.12368
Moira River near Deloro	1.983	-0.20980
Basswood River near Winton	2.008	0.00285
Black Sturgeon River at Highway No. 17	2.048	-0.00212
North Branch Muskoka River at Port Sydney	2.074	-0.20216
Moira River near Foxboro	2.075	-0.14014

Note: The rivers exhibiting dominance of the brown noise are highlighted by bolded letters.

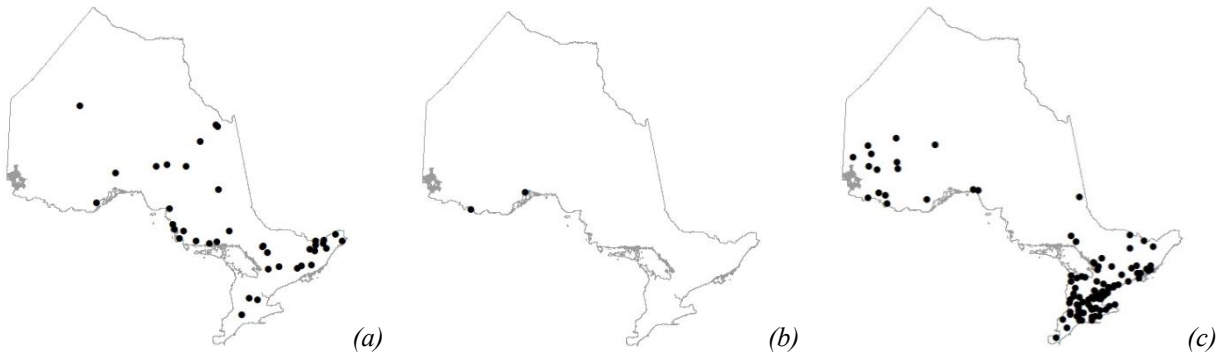

Figure 7. Distribution of stations in Ontario corresponding to the presence of: (a) pink noise, (b) brown noise, and (c) black noise.

The best-fit lines in both figures are depicted with their respective equations. It is noted that, since only two stations exhibited characteristics of brown noise, these were excluded from the analysis shown in Figure 8b, as inclusion of them would have resulted in a mean squared error (MSE) of zero. Table 3 presents various cases with their corresponding MSE values.

For the combined noise model, where all coloured noise (pink, brown, and black) is treated together, the linear fit is given by the equation $\alpha = 2.6296H + 0.8768$, with an MSE of 0.236. However, a relatively high value of MSE suggests that the equation lacks an optimal fit.

When the coloured noise is separated by pink and black noise consideration, it shows an improved best fit with lower MSE. For Pink noise, the linear relationship of $\alpha = 0.1156H + 1.6258$ with a significantly lower MSE of 0.050 was found, and for black noise, the linear model is expressed as $\alpha = 2.0396H + 1.4718$ with an MSE of 0.053.

A relatively very gradual slope of 0.1156 in the α-H relationship for pink noise indicates that the scaling exponent is less dependent on variations in the Hurst coefficient. This is suggestive of the fact that the level of pink noise remains relatively stable despite changes in the Hurst coefficient of a series. On the other hand, a sharp slope of 2.0396 in the α-H relationship for black noise is indicative of the fact that the level of black noise is highly dependent on H. Considering $0.5<H<1$, for black noise, $2.5 < \alpha < 3.5$. These findings are aligned with the fact that pink noise has lower memory than black noise.

It is noted that when streamflow data from a hydrometric station is characterized by a specific type of coloured noise, it does not imply the absence of other types of coloured noise (See: section 2.2 for additional detail). Instead, it is indicative of the fact that the characteristics of the dominant-coloured noise overshadow those of the others. When modelling such a series, it is important to consider that preserving the characteristics of one noise type (e.g., black noise) may compromise the preservation of characteristics associated with other noise types (e.g., pink noise).

Table 3. Approaches and corresponding models for fitting 'α' values as a function of the Hurst coefficient.

Case	Model (α=F(H))	MSE*
Linear fit without separating noise colour (for pink, brown, and black)	α= 2.6296H + 0.8768	0.236
Linear fit for pink noise	α = 0.1156H + 1.6258	0.050
Linear fit for black noise	α = 2.0396H + 1.4718	0.053

*Note: *MSE* $= 1/n \sum_{i=0}^{n}(\alpha_i - \hat{\alpha}_i)^2$, *where n is the number of data points,* α_i *and* $\hat{\alpha}_i$ *are respectively the actual and predicted values of α.*

Therefore, using the methodology presented in this paper suggests that a series dominated by the presence of pink noise, models from the AR family may suffice. For black noise, a model with higher memory capabilities may be necessary, while for Brownian noise, a model based on Brownian motion could prove useful. However, it is crucial for the analyst to carefully determine which coloured noise characteristics of the time series are essential to preserve the desired

properties of the time series. The user must consider the potential consequences of not retaining other noise characteristics, as such trade-offs may impact the overall model performance and effectiveness.

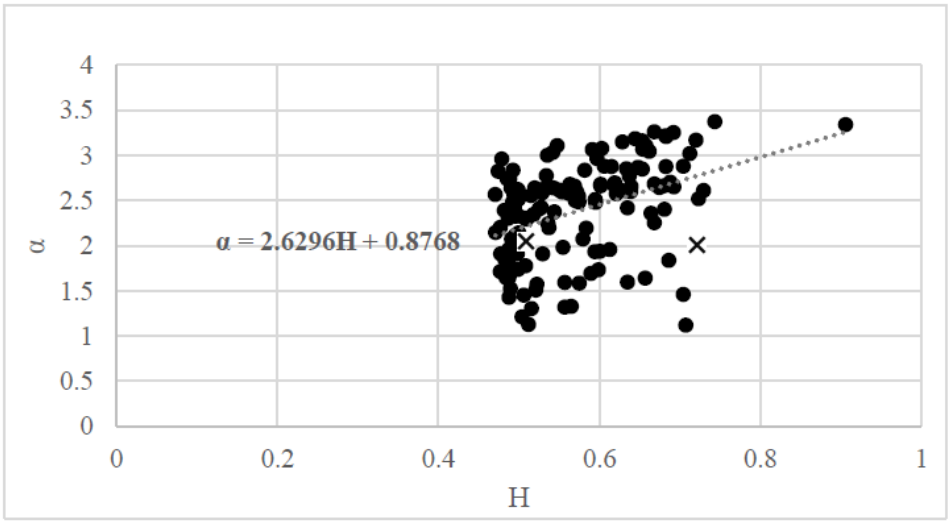

(a)

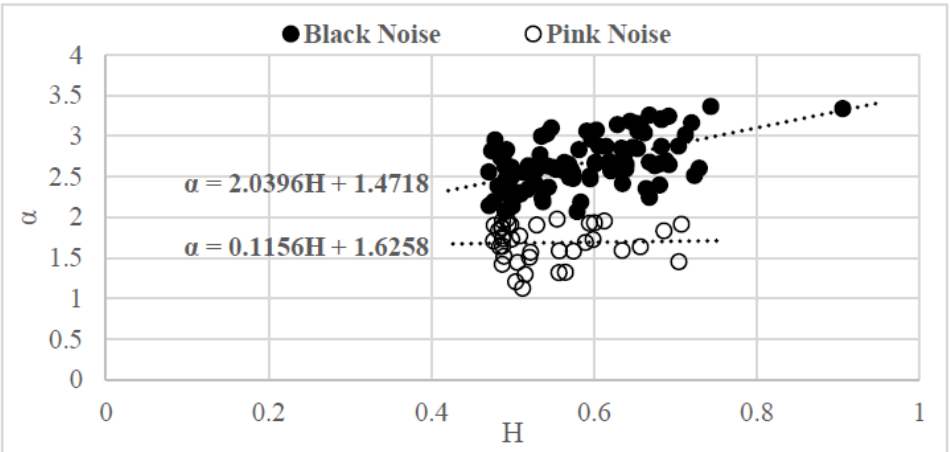

Note: In Figure 8a, the points represented by × correspond to brown noise, and hence were excluded from Figure 8b, where pink and black noise are analyzed separately and individually.

(b)

Figure 8. Hurst coefficient (H) versus scaling exponent α values for the hydrometric stations: (a) without separating different levels of noise, and (b) with noise levels separated.

4. CONCLUSION

This study simplifies the PSD analysis of monthly streamflow sequences by isolating jumps where frequencies are a fraction of a cycle (12 months). Additionally, the study explores the α-H relationship in non-stationary monthly streamflow sequences. An α-H relationship, as a function of two distinct types of noise, pink and black ($\alpha = 0.1156H + 1.6258$) and only for the black noise ($\alpha = 2.0396H + 1.4718$). It is further observed that for a higher slope of the black noise, the α-H relationship is indicative that a system is characterized by dominance of the black noise, and long-term memory plays a more significant role. In contrast, the dominance of the pink noise highlights the importance of mean-reverting characteristics in the system.

A linear model for α-H has been calibrated for Ontario, and it is recommended that similar analyses be conducted for other provinces to further enhance understanding and improve modelling accuracy across regions.

Moreover, in Ontario, jumps were observed at all fractions of a year. It might not apply to another region where fewer sub-patterns exist, and therefore, region-specific α-H relationships need to be developed.

The authors observed an increase in PSD after $f > 0.5$ in some streamflow data sets from hydrometric stations exhibited in Figure 5b and 5c for Basswood and English Rivers, respectively. Which means the PSD does not follow a power law. Additionally, jumps in PSD were observed at $f = 0.5833, 0.6667, 0.75, 0.833, 0.9167$ months^{-1} in most hydrometric stations, regardless of whether there was an overall increase in PSD for $f > 0.5$. Both the observed increase and the specific jumps in PSD for $f > 0.5$ warrant further investigations.

ETHICAL APPROVAL

Both authors hereby consent to participate. Both authors hereby consent to publish.

AUTHOR CONTRIBUTIONS

Both authors contributed to the conception and design of the study. Material preparation, data collection and analysis were performed by Shirin Studnicka (nee: Piran). The first draft of the manuscript was written by Shirin Studnicka (nee: Piran), and both authors commented on previous versions of the manuscript. Both authors read and approved the final manuscript.

FUNDING

The authors declare that no funds, grants, or other support were received during the preparation of this manuscript.

COMPETING INTERESTS

The authors have no relevant financial or non-financial interests to disclose.

AVAILABILITY OF DATA AND MATERIALS

The data sets used in the study are easily accessible from the HYDAT website maintained by Environment Canada.

APPENDIX A

Table A1. Summary of relevant information on hydrometric stations used in this study.

No	Station Name	Station Number	Location (Lat. & Long.)	Drainage Area (km^2)	Years of Records (Jan-Dec)
1	Alder Creek near New Dundee	02GA030	43° 22' 20" N 80° 33' 03" W	47.4	1970-2023
2	Ausable River near Springbank	02FF002	43° 04' 18" N 81° 39' 35" W	865	1948-2023
3	Aux Sables River at Massey	02CE002	46° 12' 53" N 82° 04' 14" W	1,340	1921-2023
4	Avon River below Stratford	02GD018	43° 20' 41" N 81° 06' 59" W	140	1965-2023
5	Basswood River near Winton	05PA012	48° 04' 57" N 91° 39' 04" W	4,510	1930-2015
6	Batchawana River near Batchawana	02BF001	47° 00' 12" N	1,230	1968-2023

7	Bayfield River near Varna	02FF007	84° 30' 56" W 43° 33' 04" N 81° 35' 22" W	460	1967-2023
8	Bear Creek near Petrolia	02GG006	42° 54' 21" N 82° 07' 08" W	249	1967-2023
9	Beaver River near Clarksburg	02FB009	44° 31' 11" N 80° 28' 04" W	587	1961-2023
10	Big Creek near Delhi	02GC006	42° 50' 15" N 80° 30' 35" W	370	1956-2023
11	Big Creek near Walsingham	02GC007	42° 41' 08" N 80° 32' 18" W	567	1956-2023
12	Big East River near Huntsville	02EB013	45° 23' 33" N 79° 09' 35" W	610	1974-2023
13	Bighead River near Meaford	02FB010	44° 34' 12" N 80° 38' 54" W	298	1958-2023
14	Black Creek near Weston	02HC027	43° 40' 27" N 79° 30' 15" W	58	1967-2023
15	Black River near Actinolite	02HL003	44° 32' 22" N 77° 22' 10" W	429	1956-2023
16	Black River near Washago	02EC002	44° 42' 49" N 79° 16' 53" W	1,510	1917-2023
17	Black Sturgeon River at Highway No. 17	02AC002	48° 54' 15" N 88° 22' 36" W	2,980	1972-2023
18	Blackwater River at Beardmore	02AD010	49° 35' 51" N 87° 57' 55" W	652	1972-2023
19	Blanche River above Englehart	02JC008	47° 53' 20" N 79° 52' 45" W	1,780	1973-2023
20	Blue Springs Creek near Eden Mills	02GA031	43° 34' 34" N 80° 06' 32" W	41.5	1966-2023
21	Bonnechere River at Castleford	02KC009	45° 29' 47" N 76° 33' 52" W	2,380	1963-2023
22	Burnt River near Burnt River	02HF003	44° 42' 35" N 78° 40' 39" W	1,250	1963-2023
23	Canagagigue Creek near Elmira	02GA023	43° 34' 47" N 80° 30' 33" W	114	1965-2023
24	Carp River near Kinburn	02KF011	45° 25' 03" N 76° 11' 55" W	258	1972-2023
25	Cat River below Wesleyan Lake	04GA002	51° 10' 25" N 91° 35' 40" W	5,390	1971-2023
26	Catfish Creek near Sparta	02GC018	42° 44' 45" N 81° 03' 25" W	295	1965-2023
27	Cedar River below Wabaskang Lake	05QE008	50° 30' 27" N 93° 15' 30" W	1,690	1970-2023
28	Chukuni River near Ear Falls	05QC001	50° 52' 25" N 93° 29' 05" W	4,920	1963-2023
29	Clyde River at Gordon Rapids	02KF013	45° 08' 02" N 76° 37' 47" W	291	1972-2023
30	Clyde River near Lanark	02KF010	45° 02' 45" N 76° 24' 03" W	618	1971-2023
31	Coldwater River at Coldwater	02ED007	44° 42' 25" N 79° 38' 37" W	168	1966-2023
32	Collins Creek near Kingston	02HM005	44° 15' 23" N 76° 36' 45" W	160	1970-2023
33	Conestogo River at Glen Allan	02GA028	43° 39' 17" N 80° 42' 07" W	571	1960-2023
34	Consecon Creek at Allisonville	02HE002	44° 01' 38" N 77° 22' 00" W	119	1970-2023
35	Credit River near Cataract	02HB001	43° 50' 09" N 80° 01' 22" W	209	1916-2023
36	Credit River near Orangeville	02HB013	43° 53' 28" N 43° 53' 28" N	60.6	1968-2023
37	Credit River West Branch at Norval	02HB008	43° 38' 47" N 79° 51' 58" W	131	1964-2023
38	Crowe River at Marmora	02HK003	44° 28' 53" N 77° 41' 05" W	1,930	1960-2023
39	Depot Creek at Bellrock	02HM002	44° 28' 18" N 76° 45' 44" W	181	1957-2023
40	Don River at Todmorden	02HC024	43° 41' 09" N 79° 21' 41" W	319	1963-2022
41	East Humber River near Pine Grove	02HC009	43° 47' 24" N	191	1954-2023

			79° 35' 03" W		
42	East Sixteen Mile Creek near Omagh	02HB004	43° 29' 57" N 79° 46' 36" W	193	1958-2023
43	English River at Umfreville	05QA002	49° 52' 24" N 91° 27' 35" W	6,230	1922-2023
44	Eramosa River above Guelph	02GA029	43° 32' 52" N 80° 10' 55" W	231	1963-2023
45	Etobicoke Creek below Queen Elizabeth Highway	02HC030	43° 36' 06" N 79° 33' 22" W	205	1967-2023
46	Fairchild Creek near Brantford	02GB007	43° 08' 50" N 80° 09' 16" W	389	1965-2015
47	French River at Dry Pine Bay	02DD010	46° 04' 06" N 80° 36' 41" W	13,900	1962-2022
48	Goulais River near Searchmont	02BF002	46° 51' 39" N 83° 58' 18" W	1,140	1968-2023
49	Grand River at Brantford	02GB001	43° 07' 57" N 80° 16' 02" W	5,200	1948-2023
50	Gull River at Norland	02HF002	44° 43' 54" N 78° 49' 05" W	1,280	1963-2023
51	Holland River East Branch at Holland Landing	02EC009	44° 05' 41" N 79° 29' 22" W	176	1966-2023
52	Humber River at Weston	02HC003	43° 41' 56" N 79° 31' 13" W	802	1949-2023
53	Indian River near Blakeney	02KF012	45° 14' 43" N 76° 15' 37" W	212	1972-2023
54	Jackson Creek at Peterborough	02HJ001	44° 18' 10" N 78° 19' 17" W	116	1963-2023
55	Jock River near Richmond	02LA007	45° 14' 57" N 75° 47' 26" W	526	1970-2023
56	Kaministiquia River at Kaministiquia	02AB006	48° 31' 56" N 89° 35' 42" W	6,470	1935-2023
57	Kemptville Creek near Kemptville	02LA006	44° 59' 39" N 75° 39' 44" W	411	1970-2023
58	Kettle Creek at St. Thomas	02GC002	42° 46' 39" N 81° 12' 50" W	331	1968-2023
59	Kwetabohigan River near the Mouth	04KA001	51° 09' 39" N 80° 51' 50" W	4,250	1973-2023
60	Little Pic River near Coldwell	02BA003	48° 50' 56" N 86° 36' 25" W	1,320	1973-2023
61	Little Rouge Creek near Locust Hill	02HC028	43° 54' 28" N 79° 12' 58" W	83.6	1964-2022
62	Little White River near Bellingham	02CC005	46° 23' 38" N 83° 16' 58" W	1,970	1943-2023
63	Lynde Creek near Whitby	02HC018	43° 52' 31" N 78° 57' 37" W	100	1976-2020
64	Lynn River at Simcoe	02GC008	42° 49' 24" N 80° 17' 22" W	144	1958-2023
65	Madawaska River at Palmer Rapids	02KD004	45° 19' 41" N 77° 30' 55" W	5,800	1930-2023
66	Maitland River above Wingham	02FE005	43° 54' 54" N 81° 15' 51" W	527	1954-2023
67	Mattagami River near Timmins	04LA002	48° 24' 15" N 81° 26' 54" W	5,570	1974-2023
68	McKenzie Creek near Caledonia	02GB010	43° 02' 02" N 79° 56' 59" W	173	1962-2023
69	Medway River in London	02GD008	43° 00' 49" N 81° 16' 49" W	203	1971-2023
70	Michipicoten River at Scott Falls	02BD002	47° 54' 38" N 84° 44' 35" W	5,310	1924-2020
71	Middle Maitland River near Belgrave	02FE008	43° 48' 46" N 81° 18' 24" W	645	1968-2023
72	Middle Maitland River near Listowel	02FE003	43° 43' 38" N 80° 58' 21" W	73.4	1954-2023
73	Middle Thames River at Thamesford	02GD004	43° 03' 32" N 80° 59' 41" W	306	1949-2023
74	Millhaven Creek near Millhaven	02HM006	44° 13' 35" N 76° 45' 32" W	144	1971-2023
75	Missinaibi River at Mattice	04LJ001	49° 36' 39" N 83° 16' 04" W	8,570	1921-2023
76	Missinaibi River below Waboose River	04LM001	50° 35' 07" N	22,900	1976-2023

			82° 05' 27" W		
77	Mississippi River at Appleton	02KF006	45° 10' 34" N 76° 07' 24" W	2,940	1919-2023
78	Moira River near Deloro	02HL005	44° 29' 59" N 77° 37' 06" W	297	1966-2023
79	Moira River near Foxboro	02HL001	44° 15' 13" N 77° 25' 07" W	2,590	1916-2023
80	Montreal River near Montreal River Harbour	02BE002	47° 12' 50" N 84° 37' 10" W	2,880	1936-2020
81	Moon River at Highway No. 400	02EB011	45° 03' 54" N 79° 47' 24" W	4,790	1966-2023
82	Musquash River at Highway No. 400	02EB012	45° 01' 21" N 79° 46' 36" W	N/A	1966-2023
83	Nagagami River at Highway No. 11	04JC002	49° 46' 22" N 84° 32' 13" W	2,180	1951-2023
84	Namakan River at the Outlet of Lac La Croix	05PA006	48° 22' 57" N 92° 10' 34" W	13,400	1923-2023
85	Nanticoke Creek at Nanticoke	02GC022	42° 48' 35" N 80° 04' 34" W	177	1970-2023
86	Napanee River at Camden East	02HM007	44° 20' 04" N 76° 50' 20" W	700	1974-2023
87	Neebing River near Thunder Bay	02AB008	48° 23' 00" N 89° 18' 23" W	187	1954-2022
88	Niagara River at Queenston	02HA003	43° 09' 25" N 79° 02' 50" W	686,000	1860-2021
89	Nith River above Nithburg	02GA038	43° 29' 02" N 80° 50' 06" W	326	1973-2023
90	Nith River near Canning	02GA010	43° 11' 23" N 80° 27' 18" W	1,030	1914-2023
91	North Branch Muskoka River at Port Sydney	02EB004	45° 12' 46" N 79° 16' 31" W	1,410	1916-2023
92	North French River near the Mouth	04MF001	51° 04' 36" N 80° 45' 50" W	6,680	1967-2023
93	North Magnetawan River above Pickerel Lake	02EA010	45° 42' 13" N 79° 18' 31" W	155	1969-2022
94	North Magnetawan River near Burk's Falls	02EA005	45° 40' 10" N 79° 22' 45" W	329	1916-2023
95	North Thames River at St. Mary’s	02GD005	43° 15' 20" N 81° 08' 44" W	1,080	1952-2023
96	North Thames River near Mitchell	02GD014	43° 27' 01" N 81° 12' 24" W	315	1914-2023
97	North Thames River near Thorndale	02GD015	43° 08' 57" N 81° 11' 31" W	1,320	1954-2023
98	Nottawasaga River near Baxter	02ED003	44° 14' 59" N 79° 49' 17" W	1,230	1950-2023
99	Ogoki River above Whiteclay Lake	04GB004	50° 52' 06" N 88° 55' 53" W	11,200	1972-2023
100	Oshawa Creek at Oshawa	02HD008	43° 55' 49" N 78° 53' 29" W	95.8	1960-2022
101	Pagwachuan River at Highway No. 11	04JD005	49° 45' 51" N 85° 13' 34" W	2,120	1968-2022
102	Parkhill Creek above Parkhill Reservoir	02FF008	43° 09' 50" N 81° 37' 53" W	113	1974-2023
103	Petawawa River near Petawawa	02KB001	45° 53' 10" N 77° 18' 55" W	4,120	1916-2022
104	Pic River near Marathon	02BB003	48° 46' 26" N 86° 17' 47" W	4,220	1971-2022
105	Pipestone River at Karl Lake	04DA001	52° 34' 50" N 90° 11' 12" W	5,960	1967-2022
106	Rainy River at Fort Frances	05PC019	48° 36' 30" N 93° 24' 12" W	38,600	1906-2022
107	Raisin River near Williamstown	02MC001	45° 09' 19" N 74° 38' 17" W	404	1961-2023
108	Rideau River at Ottawa	02LA004	45° 22' 53" N 75° 41' 49" W	3,810	1949-2023
109	Root River at Sault Ste. Marie	02CA002	46° 33' 46" N 84° 16' 54" W	109	1972-2023
110	Rouge River near Markham	02HC022	43° 51' 30" N 79° 14' 00" W	181	1962-2022
111	Ruscom River near Ruscom Station	02GH002	42° 12' 41" N	125	1972-2023

112	Salmon River near Shannonville	02HM003	82° 37' 44" W 44° 12' 26" N 77° 12' 33" W	907	1959-2023
113	Sauble River at Sauble Falls	02FA001	44° 40' 39" N 81° 15' 21" W	913	1957-2023
114	Saugeen River near Port Elgin	02FC001	44° 27' 23" N 81° 19' 35" W	3,950	1915-2023
115	Saugeen River near Walkerton	02FC002	44° 07' 13" N 81° 06' 55" W	2,140	1915-2023
116	Seine River at Sturgeon Falls Generating Station	05PB009	48° 44' 40" N 92° 17' 05" W	5,880	1964-2021
117	Serpent River at Highway No. 17	02CD001	46° 12' 38" N 82° 30' 44" W	1,350	1967-2023
118	Severn River at Swift Rapids	02EC003	44° 51' 25" N 79° 32' 30" W	5,850	1954-2021
119	Shelter Valley Brook near Grafton	02HD010	43° 59' 30" N 78° 00' 04" W	63.8	1966-2023
120	Sixteen Mile Creek at Milton	02HB005	43° 30' 50" N 79° 52' 47" W	101	1959-2023
121	Skootamatta River near Actinolite	02HL004	44° 32' 58" N 77° 19' 41" W	678	1959-2023
122	South Maitland River at Summerhill	02FE009	43° 41' 03" N 81° 32' 28" W	371	1968-2023
123	South Nation River near Plantagenet Springs	02LB005	45° 31' 01" N 74° 58' 41" W	3,810	1949-2023
124	Speed River below Guelph	02GA015	43° 32' 01" N 80° 15' 08" W	568	1951-2023
125	Speed River near Armstrong Mills	02GA040	43° 38' 19" N 80° 16' 12" W	167	1974-2023
126	Sturgeon River at McDougall Mills	05QA004	50° 10' 02" N 91° 32' 26" W	4,440	1962-2023
127	Sturgeon River at the Outlet of Salvesen Lake	05QE009	50° 21' 08" N 94° 27' 59" W	1,530	1965-2023
128	Sydenham River near Alvinston	02GG002	42° 49' 50" N 81° 51' 06" W	701	1949-2023
129	Sydenham River near Owen Sound	02FB007	44° 31' 20" N 80° 55' 48" W	183	1949-2023
130	Thames River at Byron	02GE002	42° 57' 45" N 81° 19' 54" W	3,080	1956-2023
131	Thames River at Ingersoll	02GD016	43° 02' 28" N 80° 53' 10" W	510	1958-2023
132	Thames River at Thamesville	02GE003	42° 32' 41" N 81° 58' 02" W	4,370	1956-2023
133	Thames River near Ealing	02GD001	42° 58' 24" N 81° 12' 30" W	1,340	1916-2023
134	Turtle River near Mine Centre	05PB014	48° 51' 00" N 92° 43' 25" W	4,770	1921-2023
135	Twenty Mile Creek at Balls Falls	02HA006	43° 08' 00" N 79° 22' 59" W	292	1958-2023
136	Wabigoon River at Dryden	05QD016	49° 46' 55" N 92° 50' 34" W	2,340	1971-2021
137	Wabigoon River near Quibell	05QD006	49° 57' 28" N 93° 24' 01" W	6,490	1954-2023
138	Wanapitei River near Wanup	02DB005	46° 20' 44" N 80° 50' 22" W	3,150	1953-2023
139	Welland River below Caistor Corners	02HA007	43° 01' 18" N 79° 37' 04" W	223	1958-2023
140	West Humber River at Highway No. 7	02HC031	43° 45' 30" N 79° 40' 44" W	142	1966-2023
141	Whitemans Creek near Mount Vernon	02GB008	43° 07' 34" N 80° 23' 01" W	386	1962-2023
142	Whitson River at Chelmsford	02CF007	46° 35' 00" N 81° 11' 56" W	277	1961-2023
143	Wilmot Creek near Newcastle	02HD009	43° 55' 48" N 78° 37' 07" W	80.7	1966-2022

REFERENCES

Balabana, E., & Lub, S. (2018). Colour of noise: comparative analysis of sub-periodic variation in empirical Hurst exponent across foreign currency changes and their pairwise differences. Preprint 2018. Available online: https://www.researchgate.net/profile/Shan-Lu-7/publication/328230754_Color_of_noise_Comparative_analysis_of_subperiodic_variation_in_empirical_Hurst_exponent_across_foreign_currency_changes_and_their_pairwise_differences/links/5cd0c112458515712e973d7d/Color-of-noise-Comparative-analysis-of-sub-periodic-variation-in-empirical-Hurst-exponent-across-foreign-currency-changes-and-their-pairwise-differences.pdf (accessed on 25 October 2025).

Blöschl, G., & Sivapalan, M. (1995). Scale issues in hydrological modelling: a review. Hydrological Processes, 9(3-4), 251-290.

Boes, D. C., & Salas, J. D. (1978). Nonstationarity of the mean and the Hurst phenomenon. Water Resources Research, 14(1), 135-143.

Bullmore, E., Long, C., Suckling, J., Fadili, J., Calvert, G., Zelaya, F., Carpenter, T. A., & Brammer, M. (2001). Colored noise and computational inference in neurophysiological (fMRI) time series analysis: resampling methods in time and wavelet domains. Human brain mapping, 12(2), 61-78.

Chen, X., Wang, M., Zhang, Y., Feng, Y., Wu, Z., & Huang, N. E. (2013). Detecting signals from data with noise: theory and applications. Journal of the Atmospheric Sciences, 70(5), 1489-1504.

Cuddington, K. M., & Yodzis, P. (1999). Black noise and population persistence. Proceedings of the Royal Society of London. Series B: Biological Sciences, 266(1422), 969-973.

Dolgonosov, B., Korchagin, K., & Kirpichnikova, N. (2008). Modelling of annual oscillations and 1/f-noise of daily river discharges. Journal of Hydrology, 357(3-4), 174-187.

Dooley, K. J., & Van de Ven, A. H. (1997). A primer on diagnosing dynamic organizational processes. Strategic Management Research Center, University of Minnesota, MN, USA. Available online: https://scholar.google.com/scholar_lookup?title=A+Primer+on+Diagnosing+Dynamic+Organizational+Processes&author=Dooley,+K.J.&author=Van+de+Ven,+A.H.&publication_year=1997.

Fiering, M. B., & Bund, B. (1971). Synthetic streamflows (Vol. 1). American Geophysical Union, Washington, DC, USA.

Gallant, J. C., Moore, I. D., Hutchinson, M. F., & Gessler, P. (1994). Estimating fractal dimension of profiles: a comparison of methods. Mathematical Geology, 26, 455-481.

Gu, X., Sun, H., Tick, G. R., Lu, Y., Zhang, Y., Zhang, Y., & Schilling, K. (2020). Identification and scaling behavior assessment of the dominant hydrological factors of nitrate concentrations in streamflow. Journal of Hydrologic Engineering, 25(6), 06020002.

Hurst, H. E. (1951). Long-term storage capacity of reservoirs. Transactions of the American society of civil engineers, 116(1), 770-799.

Jackson, B. B. (1975). The use of streamflow models in planning. Water Resources Research, 11(1), 54-63.

Kim, D. H., Rao, P. S. C., Kim, D., & Park, J. (2016). 1/f noise analyses of urbanization effects on streamflow characteristics. Hydrological Processes, 30(11), 1651-1664.

Klemeš, V. (1974). The Hurst phenomenon: A puzzle? Water Resources Research, 10(4), 675-688.

Koirala, S. R., Gentry, R. W., Perfect, E., Mulholland, P. J., & Schwartz, J. S. (2011). Hurst analysis of hydrologic and water quality time series. Journal of Hydrologic Engineering, 16(9), 717-724.

Koscielny-Bunde, E., Kantelhardt, J. W., Braun, P., Bunde, A., & Havlin, S. (2006). Long-term persistence and multifractality of river runoff records: Detrended fluctuation studies. Journal of Hydrology, 322(1-4), 120-137.

Koutsoyiannis, D. (2003). Climate change, the Hurst phenomenon, and hydrological statistics. Hydrological Sciences Journal, 48(1), 3-24.

Legates, D. R., & Outcalt, S. I. (2022). Detection of climate transitions and discontinuities by Hurst rescaling. International Journal of Climatology, 42(9), 4753-4772.

Livina, V., Kizner, Z., Braun, P., Molnar, T., Bunde, A., & Havlin, S. (2007). Temporal scaling comparison of real hydrological data and model runoff records. Journal of Hydrology, 336(1-2), 186-198.

Markonis, Y., Moustakis, Y., Nasika, C., Sychova, P., Dimitriadis, P., Hanel, M., Máca, P., & Papalexiou, S. (2018). Global estimation of long-term persistence in annual river runoff. Advances in Water Resources, 113, 1-12.

Panu, U. S., & Unny, T. (1980a). Extension and application of the feature prediction model for the synthesis of hydrologic records. Water Resources Research, 16(1), 77-96.

Panu, U. S., & Unny, T. (1980b). Stochastic synthesis of hydrologic data based on concepts of pattern recognition: I. General methodology of the approach. Journal of Hydrology, 46(1-2), 5-34.

Panu, U. S., & Unny, T. (1980c). Stochastic synthesis of hydrologic data based on concepts of pattern recognition: II. Application of natural watersheds. Journal of Hydrology, 46(3-4), 197-217.

Piran, S., & Panu, U. (2023). Encoded-Streamflow Synthesis using Textural Feature Recognition System. AGU Fall Meeting Abstracts, H44G-03c,

Rhif, M., Ben Abbes, A., Farah, I. R., Martínez, B., & Sang, Y. (2019). Wavelet transform application for/in non-stationary time-series analysis: A review. Applied Sciences, 9(7), 1345.

Rodriguez-Iturbe, I., & Rinaldo, A. (1997). Fractal river basins: chance and self-organization. Cambridge University Press: Cambridge, UK.

Salas, J. D., Delleur, J. W., Yevjevich, V., & Lane, W. L. (1980). Applied modelling of hydrologic time series. Water Resources Publication, Littleton, Colorado, USA.

Sharma, A., Tarboton, D. G., & Lall, U. (1997). Streamflow simulation: A nonparametric approach. Water Resources Research, 33(2), 291-308.

Souza, V., & Assireu, A. (2016). Detrended fluctuation analysis of spatially extended digital surfaces: the classification process of 1/f noise and computational performance. J. Comput. Interdiscip. Sci, 24, 25.

Stedinger, J. R., & Taylor, M. R. (1982). Synthetic streamflow generation: 1. Model verification and validation. Water Resources Research, 18(4), 909-918.

Stoyanov, M., Gunzburger, M., & Burkardt, J. (2011). Pink noise, 1/f α noise, and their effect on solutions of differential equations. International journal for uncertainty quantification, 1(3).

Studnicka, S., & Panu, U. (2025). Streamflow Synthesis Using an Encoded Textural Pattern Recognition System. II: Model Applications. Journal of Hydrologic Engineering, 30(6), 04025040.

Suman, A., Devarajan Sindhu, A., Nayak, A. K., Sankaran Namboothiri, A., & Biswal, B. (2023). Unveiling the climatic origin of streamflow persistence through multifractal analysis of hydro-meteorological datasets of India. Hydrological Sciences Journal, 68(2), 290-306.

Sun, J., Zhao, Y., Zhang, J., Luo, X., & Small, M. (2007). Reducing colored noise for chaotic time series in the local phase space. Physical Review E—Statistical, Nonlinear, and Soft Matter Physics, 76(2), 026211.

Szolgayova, E., Laaha, G., Blöschl, G., & Bucher, C. (2014). Factors influencing long-range dependence in streamflow of European rivers. Hydrological Processes, 28(4), 1573-1586.

Telesca, L., Lovallo, M., Lopez-Moreno, I., & Vicente-Serrano, S. (2012). Investigation of scaling properties in monthly streamflow and Standardized Streamflow Index (SSI) time series in the Ebro basin (Spain). Physica A: Statistical Mechanics and its Applications, 391(4), 1662-1678.

Thompson, S. E., & Katul, G. G. (2012). Multiple mechanisms generate Lorentzian and 1/fα power spectra in daily stream-flow time series. Advances in Water Resources, 37, 94-103.

Wen, H., & Liu, Z. (2016). Separating fractal and oscillatory components in the power spectrum of a neurophysiological signal. Brain topography, 29, 13-26.

Zhang, Q., Xu, C.-Y., Yu, Z., Liu, C.-L., & Chen, Y. D. (2009). Multifractal analysis of streamflow records of the East River basin (Pearl River), China. Physica A: Statistical Mechanics and its Applications, 388(6), 927-934.